AD-A187 196 EXPERIMENTAL SET-UP AND MATHEMATICAL MODELING OF H-SHAPED BEAM TYPE STRUCTURE(U) AIR FORCE INST OF TECH WRIGHT-PATTERSON AFB OH A K JARRELL 1986 1/1

UNCLASSIFIED AFIT/CI/NR-87-82T F/G 13/13 NL

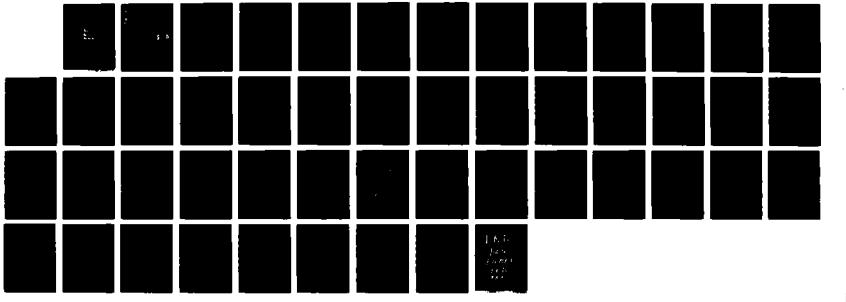

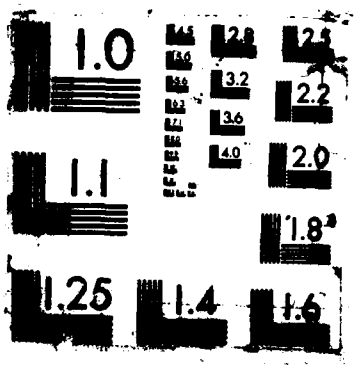
1.0
1.1
1.25
1.4
1.6
1.8
2.0
2.2
2.8
3.2
3.6
4.0

UNCLASSIFIED
SECURITY CLASSIFICATION OF THIS PAGE (When Data Entered)

## REPORT DOCUMENTATION PAGE

READ INSTRUCTIONS BEFORE COMPLETING FORM

1. REPORT NUMBER: AFIT/CI/NR 87-82T
2. GOVT ACCESSION NO.:
3. RECIPIENT'S CATALOG NUMBER:

4. TITLE (and Subtitle): Experimental Set-Up and Mathematical Modeling of H-Shaped Beam Type Structure
5. TYPE OF REPORT & PERIOD COVERED: THESIS/DISSERTATION
6. PERFORMING ORG. REPORT NUMBER:

7. AUTHOR(s): Allen K. Jarrell
8. CONTRACT OR GRANT NUMBER(s):

9. PERFORMING ORGANIZATION NAME AND ADDRESS: AFIT STUDENT AT: North Carolina State University
10. PROGRAM ELEMENT, PROJECT, TASK AREA & WORK UNIT NUMBERS:

11. CONTROLLING OFFICE NAME AND ADDRESS: AFIT/NR, WPAFB OH 45433-6583
12. REPORT DATE: 1986
13. NUMBER OF PAGES: 38

14. MONITORING AGENCY NAME & ADDRESS (if different from Controlling Office):
15. SECURITY CLASS. (of this report): UNCLASSIFIED
15a. DECLASSIFICATION/DOWNGRADING SCHEDULE:

16. DISTRIBUTION STATEMENT (of this Report)

APPROVED FOR PUBLIC RELEASE; DISTRIBUTION UNLIMITED



17. DISTRIBUTION STATEMENT (of the abstract entered in Block 20, if different from Report)

18. SUPPLEMENTARY NOTES

APPROVED FOR PUBLIC RELEASE: IAW AFR 190-1

LYNN E. WOLAVER 23 OCT 87
Dean for Research and Professional Development
AFIT/NR

19. KEY WORDS (Continue on reverse side if necessary and identify by block number)

20. ABSTRACT (Continue on reverse side if necessary and identify by block number)

ATTACHED

DD FORM 1 JAN 73 1473 EDITION OF 1 NOV 65 IS OBSOLETE

SECURITY CLASSIFICATION OF THIS PAGE (When Data Entered)

## ABSTRACT

JARRELL, ALLEN K. Experimental Set-Up and Mathematical Modeling of H-Shaped Beam Type Structure. (Under the direction of DR. LARRY M. SILVERBERG.)

An experimental set-up for a flexible H-beam type structure is designed to demonstrate flexible body maneuvers. The equations of motion for the structure are developed using the finite-element method. The H-beam is sized by looking at the structural flexibility in the system's response. Specifications necessary for the hardware used in the experiment are given.

# EXPERIMENTAL SET-UP AND MATHEMATICAL MODELING OF H-SHAPED BEAM TYPE STRUCTURE

by

ALLEN K. JARRELL

A thesis submitted to the Graduate Faculty of
North Carolina State University
in partial fulfillment of the
requirements for the Degree of
Master of Science

DEPARTMENT OF MECHANICAL AND AEROSPACE ENGINEERING

RALEIGH

1 9 8 6

APPROVED BY:

_____ _____

_____
Chairman of Advisory Committee

# BIOGRAPHY

The author was born in Norfolk, Virginia, on September 5, 1960. In June, 1978, he enrolled at the United States Air Force Academy where he received a Bachelor of Science degree in Engineering Sciences. In September, 1983, he enrolled at the University of Southern California where he received a Master of Science degree in Systems Management. He is presently working towards a Master of Science degree in Aerospace Engineering at North Carolina State University.

The author is a Captain in the United States Air Force. His first tour of duty has been as a satellite vehicle manager and contract manager for the Deputy for Defense Satellite Communications System at the United States Air Force Space Division in Los Angeles, California.

# ACKNOWLEDGEMENTS

The author wishes to express his deep appreciation to Professor Larry Silverberg, Chairman of his Advisory Committee, for his continuing guidance and support throughout the course of his studies.

Thanks are also due to the other members of his Advisory Committee, Professors R. Keltie and D. Garoutte.

Finally, the author acknowledges the support and assistance in technical editing given by Mrs. Harietta Jarrell Eley, his mother and to Mrs. Joyce Pollard for the typing of the thesis.

# TABLE OF CONTENTS

# LIST OF TABLES

# LIST OF FIGURES

# NOMENCLATURE

| | |
|---|---|
| $C$ | Constant matrix |
| $\underset{\sim}{F}(t)$ | System force vector |
| $\underset{\sim}{F}_d(t)$ | Disjointed force vector |
| $\underset{\sim}{F}_E(t)$ | Element force vector |
| $\underset{\sim}{F}_i(t)$ | Beam force vector |
| $f_r(t)$ | Modal force |
| $K$ | System stiffness matrix |
| $K_d$ | Disjointed mass matrix |
| $K_E$ | Element stiffness matrix |
| $K_i$ | Beam stiffness matrix |
| $M$ | System mass matrix |
| $M_d$ | Disjointed mass matrix |
| $M_E$ | Element mass matrix |
| $M_i$ | Beam mass matrix |
| $\underset{\sim}{u}(t)$ | Nodal displacement vector |
| $u_d(t)$ | Disjoint displacement vector |
| $\underset{\sim}{u}_E(t)$ | Element displacement vector |
| $\underset{\sim}{u}_i(t)$ | Beam displacement vector |
| $\underset{\sim}{u}_r(t)$ | Modal displacement |

Greek Symbols

| | |
|---|---|
| $\delta(t)$ | Delta function |
| $\delta_{rs}$ | Kroenecker delta function |
| $\lambda$ | Eigenvalue |
| $\lambda_r$ | Distinct eigenvalue |

| | |
|---|---|
| $\omega$ | Natural frequency |
| $\omega_r$ | Distinct natural frequency |
| $\underset{\sim}{\phi}$ | Eigenvector |
| $\underset{\sim}{\phi}_r$ | Distinct eigenvector |
| $\hat{\phi}_r$ | Normalized eigenvector |
| $< >$ | Inner product |

# 1. INTRODUCTION

Recent developments in the control of flexible structures have created the need to experimentally demonstrate the maneuver of flexible structures. In this thesis, an experimental set-up for a flexible H-beam type structure is designed (Figure 1).

The H-beam model is designed to meet several objectives. First, because the model will be used to demonstrate flexible body maneuver, the H-beam is required to possess significant structural flexibility. Secondly, the model must maneuver about three degrees of freedom. Therefore, the structure will hang from a cable and hinge attachment at the center of gravity of the H-beam. Furthermore, the cable must be of significant length in order to make the pendulum effect on the model negligible. Sizing considerations are addressed so that little, if any, static deflection (less than .01 inches) or torsional deformation results.

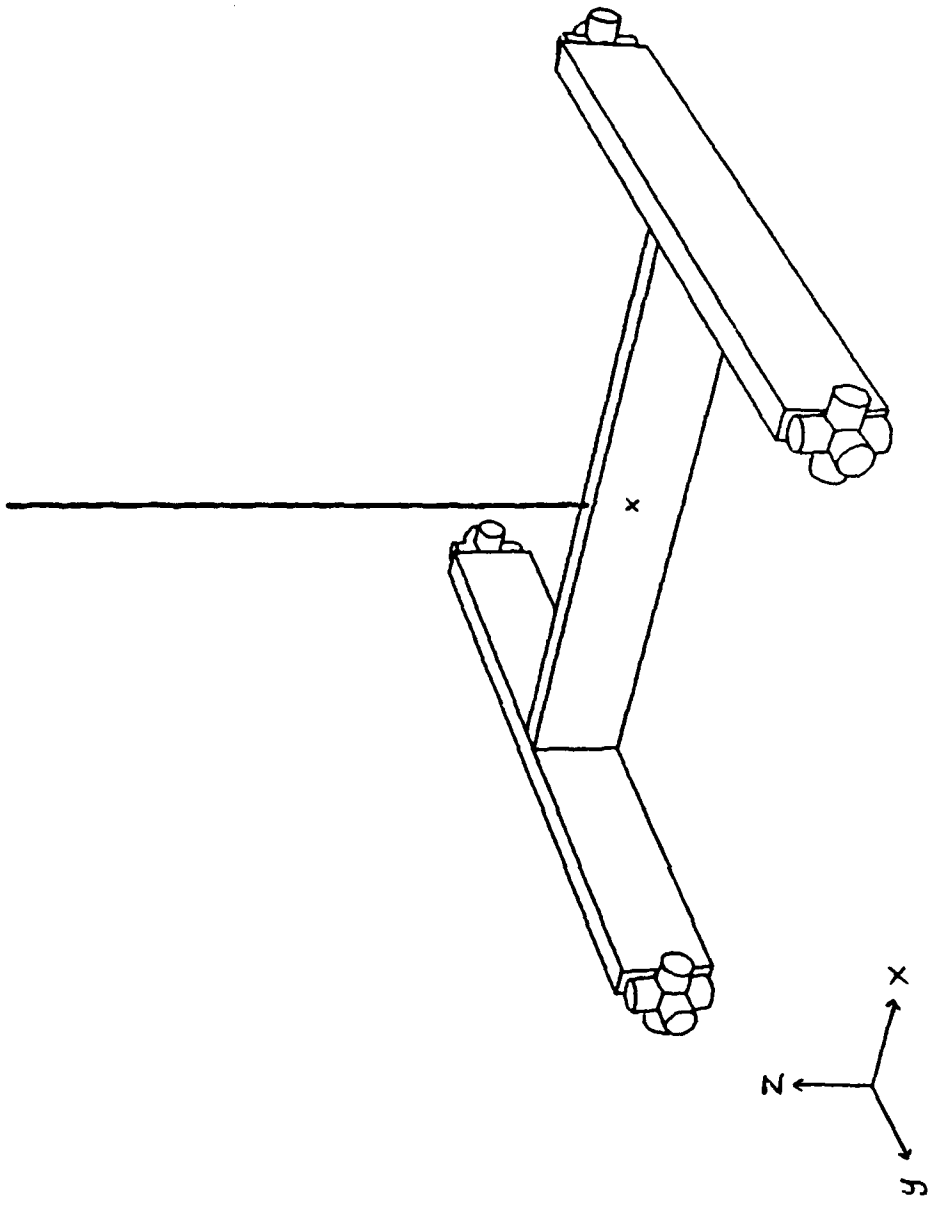


Figure 1. Diagram of H-Beam

## 2. DEVELOPMENT OF EQUATIONS OF MOTION OF STRUCTURE

The equations of motion for the H-beam are derived using the finite element method. The equations of motion for each element are given by

$$M_E \underset{\sim}{\ddot{u}}_E(t) + K_E \underset{\sim}{u}_E(t) = \underset{\sim}{F}_E(t) \tag{1}$$


Figure 2. Finite Element

where $M_E$ and $K_E$ are the element mass and stiffness matrices, respectively, for axial and transverse deformation (Ref. 1). For axial vibration, linear interpolation functions are used. Cubic interpolation functions are used for bending vibration. The element displacement vector is denoted by $\underset{\sim}{u}_E(t)$, and the element forces and element moments acting at the 2 nodes of the element are denoted by $\underset{\sim}{F}_E(t)$. The element equations of motion are used to construct the equations of motion for the three beams comprising the H-beam structure.

The equations of motion for each beam are given by

$$M_i \underset{\sim}{\ddot{u}}_i(t) + K_i \underset{\sim}{u}_i(t) = \underset{\sim}{F}_i(t) \qquad (i = 1,2,3) \tag{2}$$

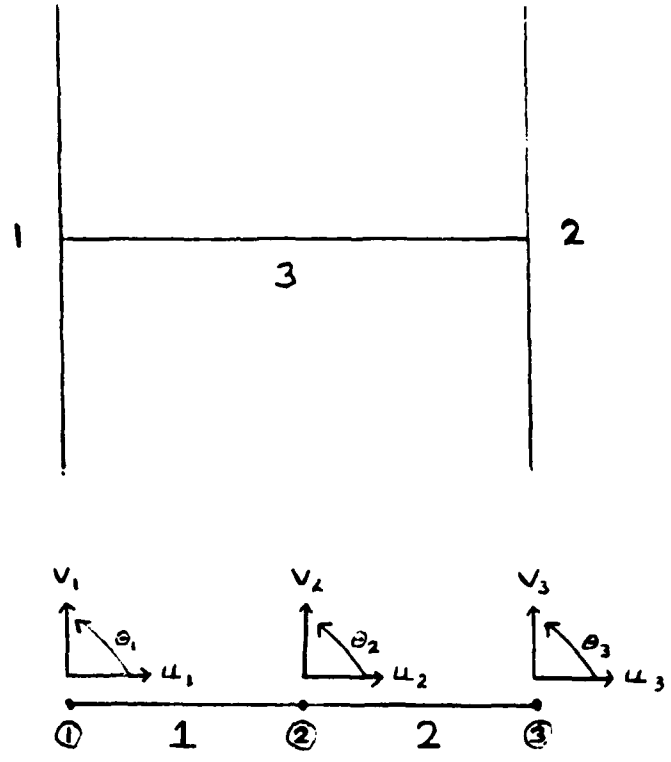


Figure 3. Beams Comprising H-Structure and a Beam Made of 2 Finite Elements

where $M_i$ and $K_i$ are the mass and stiffness matrices, respectively, for the ith beam, and $\underset{\sim}{F}_i(t)$ and $\underset{\sim}{u}_i(t)$ denote the beam force vector and the beam displacement vector, respectively. The disjointed equations of motion for the structure, Equations (2), can be expressed compactly as

$$M_d \, \ddot{\underset{\sim}{u}}_d(t) + K_d \, \underset{\sim}{u}_d(t) = \underset{\sim}{F}_d(t) \tag{3}$$

where:

$$M_d = \begin{bmatrix} M_1 & 0 & 0 \\ 0 & M_2 & 0 \\ 0 & 0 & M_3 \end{bmatrix} \qquad K_d = \begin{bmatrix} K_1 & 0 & 0 \\ 0 & K_2 & 0 \\ 0 & 0 & K_3 \end{bmatrix}$$

in which $\underset{\sim}{u}_d(t)$ and $\underset{\sim}{F}_d(t)$ denote the disjoint displacement vector and the disjoint force vector, respectively, given by

$$\underset{\sim}{u}_d(t) = \begin{Bmatrix} \underset{\sim}{u}_1(t) \\ \underset{\sim}{u}_2(t) \\ \underset{\sim}{u}_3(t) \end{Bmatrix} \qquad \underset{\sim}{F}_d(t) = \begin{Bmatrix} \underset{\sim}{F}_1(t) \\ \underset{\sim}{F}_2(t) \\ \underset{\sim}{F}_3(t) \end{Bmatrix} .$$

The three beam displacement vectors comprise $\underset{\sim}{u}_d(t)$ and the three beam force vectors comprise $\underset{\sim}{F}_d(t)$.

The transition from the local coordinates of the disjointed system to the global coordinates of the structure is accomplished using the constraint matrix C which also accounts for additional constraints placed on the structure not previously considered. In particular, it is of interest to satisfy the constraints imposed at the boundaries of the elements and to redefine the resulting displacement vector in global coordinates. To that end, the disjoint displacement vector is related to the nodal displacement vector by

$$\underset{\sim}{u}_d(t) = C\ \underset{\sim}{u}(t) \tag{4}$$

where $\underset{\sim}{u}(t)$ is the nodal displacement vector. The dimension of the displacement vector is identical to the number of degrees of freedom of the system.

The system equations of motion for the structure are obtained from the disjointed equations of motion by substituting Equation (4) into Equation (3) and premultiplying by the transpose of the constraint matrix to obtain the system equations of motion

$$M \underset{\sim}{\ddot{u}}(t) + K \underset{\sim}{u}(t) = \underset{\sim}{F}(t) \tag{5}$$

in which

$$M = C^T M_d C \quad , \qquad K = C^T K_d C \quad . \tag{6}$$

The mass matrix M and the stiffness matrix K are both symmetric n x n matrices and $\underset{\sim}{F}(t)$ denotes the system force vector

$$\underset{\sim}{F}(t) = C^T \underset{\sim d}{F}(t) \quad .$$

In assembling the equations of motion for the H-beam, it is assumed that the axial deformation along the three beams are due only to rigid-body deflections (Figure 4).

Associated with the equations of motion of the structure, the eigenvalue problem is defined as

$$\lambda M \underset{\sim}{\phi} = K \underset{\sim}{\phi} \quad . \tag{7}$$

The solution to the eigenvalue problem, referred to as the eigensolution, is comprised of the eigenvector $\underset{\sim}{\phi}$ and its associated eigenvalue $\lambda$. The matrices used in this problem are symmetric n x n; thus, there are n linearly independent eigenvectors $\underset{\sim r}{\phi}$ (r = 1,2,...,n) and n associated eigenvalues $\lambda_r$ (r = 1,2,...,n). The eigenvectors are often called the natural modes of vibration or mode shapes. The eigenvalues are related to the structure's natural frequencies $\omega_r$ by $\lambda_r = \omega_r^2$ (r = 1,2,...,n).

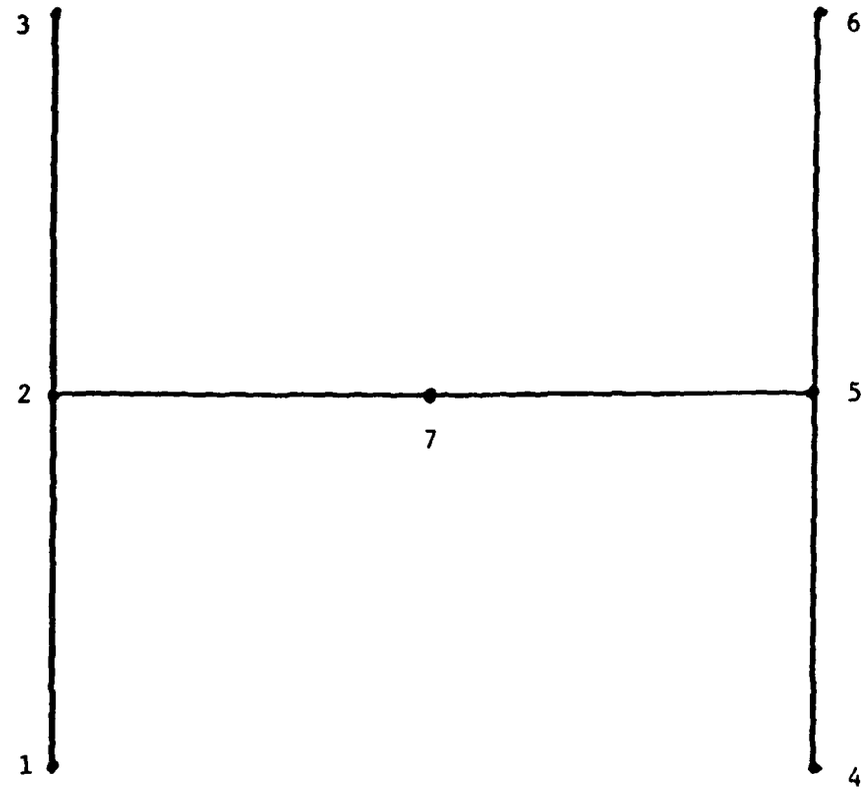


Axial Rigid-Body Deflections

$$y_1 = y_2 = y_3$$

$$y_4 = y_5 = y_6$$

$$x_2 = x_7 = x_5$$


Figure 4. Six-Element Model of H-Beam

The lower eigenvalues can be computed accurately although the computed eigensolutions with higher eigenvalues are grossly in error. This error is inherant in the discretization process that takes place in the modeling of the structure (Ref. 1). Fortunately, the errors are not important provided only the lower modes contribute significantly to the system response.

The numerical solution of the eigenvalue program is obtained for the eigenvalue problem in the form

$$\lambda \underset{\sim}{\phi} = A \underset{\sim}{\phi} \quad . \tag{8}$$

Equation (7) must be manipulated into the form of Equation (8). Equation (7) premultipling by $M^{-1}$, the inverse system mass matrix, yields Equation (8) in which $A = M^{-1}K$. Associated with Equation (8), the orthonormality conditions are in the form

$$\underset{\sim}{\phi}_r^T \underset{\sim}{\phi}_s = \delta_{rs} \tag{9}$$

$$\underset{\sim}{\phi}_r^T A \underset{\sim}{\phi}_s = \lambda_r \delta_{rs} \tag{10}$$

where $\delta_{rs}$ is the Kronecker delta function in which $\delta_{rs} = 0$ for $r \neq s$ and $\delta_{rr} = 1$. The interest lies in normalizing the eigenvectors with respect to the mass matrix M, such that

$$\underset{\sim}{\phi}_r^T M \underset{\sim}{\phi}_s = \delta_{rs} \tag{11}$$

$$\underset{\sim}{\phi}_r^T K \underset{\sim}{\phi}_s = \lambda_r \delta_{rs} \quad . \tag{12}$$

The rigid-body modes of the H structure are linearly independent and require orthonormalization. To that end, the Gram-Schmidt orthogonalization process is used to orthogonalize the eigenvectors and to normalize the eigenvectors with respect to the mass matrix (Refs. 1,8).

The nodal displacement vector $\underset{\sim}{u}(t)$ is a linear combination of the modes and written in the form

$$\underset{\sim}{u}(t) = \sum_{r=1}^{n} \underset{\sim}{\phi}_r \, u_r(t) \tag{13}$$

where $u_r(t)$ $(r = 1,2,\ldots,n)$ are modal displacements which express the extent to which each mode contributes to the overall system response. In general higher modes do not significantly participate in the response so they can be excluded from Equation (13). The modal displacements are governed by the scalar equations

$$\ddot{u}_r(t) + \omega_r^2 \, u_r(t) = f_r(t) \quad (r = 1,2,\ldots,s) \tag{14}$$

where $s << n$ and the modal forces $f_r(t)$ are related to the nodal force vector $\underset{\sim}{F}(t)$ by

$$f_r(t) = \underset{\sim}{\phi}_r^T \underset{\sim}{F}(t) \quad (r = 1,2,\ldots,s) \quad . \tag{15}$$

It remains to compute the modal displacements in Equation (14). To compute these modal displacements, the rigid-body responses and flexible-body responses must be distinguished. Because impulse forces are the type of modal forces used on the structure, new initial conditions are also calculated.

## 2.1. Rigid-Body Modal Responses ($\omega_r = 0$)

Equation (14) now has the form

$$\ddot{u}_r(t) = f_r(t) \qquad (r = 1,2,\ldots,m) \quad . \tag{16}$$

The H-beam structure is initially at rest so that

$$u_r(0) = 0 \qquad\qquad \dot{u}_r(0) = 0 \quad .$$

The nodal force vector $\underset{\sim}{F}(t)$ is expressed in the form of an impulse as

$$\underset{\sim}{F}(t) = \underset{\sim o}{F}\, \delta(t) \quad . \tag{17}$$

The rigid-body response is computed by first substituting for the modal forces $f_r(t)$ in Equation (14)

$$\ddot{u}_r(t) = \underset{\sim r}{\phi}^T \underset{\sim o}{F}\, \delta(t) \quad .$$

Introducing Equation (17) into Equations (15) and (16) and integrating over the time of the impulse from 0 to $0^+$, yields

$$\int_0^{0^+} \ddot{u}_r(t)\, dt = \underset{\sim r}{\phi}^T \underset{\sim o}{F} \int_0^{0^+} \delta(t)\, dt$$

$$\dot{u}_r(t) \Big|_0^{0^+} = \underset{\sim r}{\phi}^T \underset{\sim o}{F} \quad .$$

The new initial conditions, denoted by $\dot{u}_{ro}$ and $u_{ro}$, become

$$\dot{u}_{ro} = \dot{u}_r(0^+) = \underset{\sim r}{\phi}^T \underset{\sim o}{F} \qquad\qquad u_{ro} = u_r(0^+) = 0 \quad . \tag{18}$$

Equation (16) is now replaced with the homogeneous system

$$\ddot{u}_r(t) = 0 \quad . \tag{19}$$

Integrating Equation (19), we obtain

$$u_r(t) = At + B \qquad \dot{u}_r(t) = A$$

where the constants A and B are found using the new initial conditions as follows

$$u_{ro} = u_r(0^+) = 0 = B \qquad \dot{u}_{ro} = \dot{u}_r(0^+) = \underset{\sim}{\phi}_r^T \underset{\sim}{F}_o = A \quad . \tag{20}$$

The rigid-body response is

$$u_r(t) = \dot{u}_{ro} t \quad (r = 1,2,\ldots,m) \quad . \tag{21}$$

## 2.2. Flexible-Body Modal Responses ($\omega_r \neq 0$)

The new initial conditions due to impulse nodal forces are computed using the same integration scheme that found $\dot{u}_{ro}$ and $u_{ro}$ for the rigid-body responses. Thus, Equation (14) is integrated with respect to time from 0 to $0^+$, so that

$$\int_0^{0^+} \ddot{u}_r(t)\, dt + \omega_r^2 \int_0^{0^+} u_r(t)\, dt = \underset{\sim}{\phi}_r^T \underset{\sim}{F}_o \int_0^{0^+} \delta(t)\, dt \quad .$$

$$\dot{u}_r(t) \Big|_0^{0^+} = \underset{\sim}{\phi}_r^T \underset{\sim}{F}_o \quad .$$

The new initial conditions are given by

$$\dot{u}_{ro} = \dot{u}_r(0^+) = \underset{\sim}{\phi}_r^T \underset{\sim}{F}_o \qquad u_{ro} = u_r(0^+) = 0 \quad .$$

Equation (14) is replaced with the homogeneous system

$$\ddot{u}_r(t) + \omega_r^2 u_r(t) = 0 \quad .$$

The homogeneous solution has the form

$$u_r(t) = A_r \cos(\omega_r t) + B_r \sin(\omega_r t)$$

$$\dot{u}_t(t) = - A_r\omega_r \sin(\omega_r t) + B_r\omega_r \cos(\omega_r t)$$

where constants $A_r$ and $B_r$ are obtained using the new initial conditions

$$u_{ro} = u_r(0^+) = 0 = A_r \qquad \dot{u}_{ro} = \dot{u}_r(0^+) = \underset{\sim}{\phi}_r^T \underset{\sim}{F}_o = \omega_r B_r$$

$$B_r = \dot{u}_{ro}/\omega_r = \underset{\sim}{\phi}_r^T \underset{\sim}{F}_o/\omega_r \quad .$$

The flexible-body response can be expressed as

$$u_r(t) = \frac{\dot{u}_{ro}}{\omega_r} \sin(\omega_r t) \quad (r = m+1, m+2, \ldots, n) \quad . \tag{22}$$

The total modal response of the H-beam is the sum of the rigid-body responses and flexible-body responses. Introducing Equations (21) and (22) into Equation (13), yields

$$\underset{\sim}{u}(t) = \sum_{r=1}^{m} \underset{\sim}{\phi}_r \dot{u}_{ro} t + \sum_{m+1}^{n} \underset{\sim}{\phi}_r \frac{\dot{u}_{ro}}{\omega_r} \sin(\omega_r t) \quad . \tag{23}$$

The finite element code created models the H-beam accurately and the accuracy is shown by comparing the natural frequencies of a six-element model with a twelve-element model. The comparison shows the natural frequencies converging and the inclusion principle resulting. To test the nodal response accuracy, the six-element model is excited

by two equal and opposite impulse forces (.6 lbs each) applied at opposite ends of the structure (see Figure 5). The response at the various nodes of the model are as expected; therefore, knowing that there is a good mathematical model, the H-beam can now be dimensionalized.

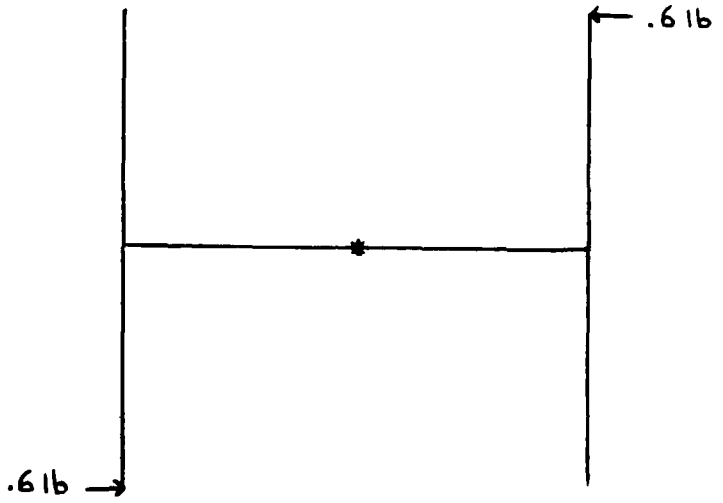


Figure 5. H-Beam Struck with 2 Impulse Forces

Table 1. Convergence and Inclusion Principle of Natural Frequencies for 6-Element and 12-Element Models

| | | | | | | | | | | | |
|---|---|---|---|---|---|---|---|---|---|---|---|
| 6-Element Model | 0.0 | | 0.0 | | 0.0 | | 24.927 | | 43.278 | | 62.151 |
| 12-Element Model | 0.0 | 0.0 | 0.0 | 24.6 | 42.8 | 61.5 | 80.1 | 98.7 | 121.1 | 187.6 | 292.6 |

| | | | | | | | | | |
|---|---|---|---|---|---|---|---|---|---|
| 6-Element Model | 82.113 | | 127.81 | | 301.85 | | 387.07 | | 570.78 |
| 12-Element Model | 337.3 | 359.1 | 373.2 | 396.5 | 424.7 | 469.2 | 512.7 | 554.6 | 593.9 |

| | | | | | | | |
|---|---|---|---|---|---|---|---|
| 6-Element Model | 612.36 | | 676.29 | | 1073.0 | | 1254.7 |
| 12-Element Model | 650.2 | 724.8 | 892.1 | 1112 | 1173 | 1317 | 1757 |

# 3. SIZING CONSIDERATIONS

The static deflection of a cantilever beam is considered for the sizing of the beam (Ref. 9). For a specific beam composition, aluminum for example, we let the static deflection in the z direction is equal to 0.01 inch, and the weight of the thrusters is equal to eight pounds thus, the beam's length can now be calculated for a specific beam cross section (see Table 2). The equation below is used to compute the beam's length

$$Z_{ST} = \frac{PL^3}{3EI} + \frac{qL^4}{8EI} \quad . \tag{24}$$

For an aluminum beam, the following values are given

$$E = 10 \times 10^6 \text{ psi} \qquad Z_{ST} = 0.01 \text{ in}$$

$$\rho = .0975 \text{ lb/in}^3 \qquad P = 8 \text{ lbs}$$

$$q = \rho bh \qquad I = \frac{1}{12} bh^3$$

where E denotes the modulus of elasticity (Young's modulus) for aluminum, $\rho$ refers to the density of aluminum, $Z_{ST}$ represents the static deflection in the z direction, I denotes the moment of inertia of the segment, P represents the weight of the thruster assembly, q refers to the weight per unit length of the segment, and L denotes the length of the segment. The length and cross section that yield the best combination of rigid-body and flexible-body displacements in the response plot are the design measurements for the segment (see Figures 6, 7, and 8). The beam will have the same cross section and twice the length of the segment. Next, the horizontal beam, connecting the two parallel beams, must be sized.

Table 2. Parallel Beams Sizing Table

| h x b | I | q | L | P |
|---|---|---|---|---|
| in x in | $in^4$ | lb/in | in | lb |
| 5 x 3 | 31.25 | 1.4625 | 60,61 | 10.5,8 |
| 5 x 2 | 20.83 | .975 | 60 | 7 |
| 5 x 1 | 10.41 | .4875 | 60,56 | 3.5,8.0 |
| 4 x 1 | 5.33 | .39 | 50 | 5.49 |
| 4 x 1.5 | 8. | .585 | 50 | 8.23 |
| 6 x 1 | 18. | .585 | 60,63 | 11.8,8.0 |

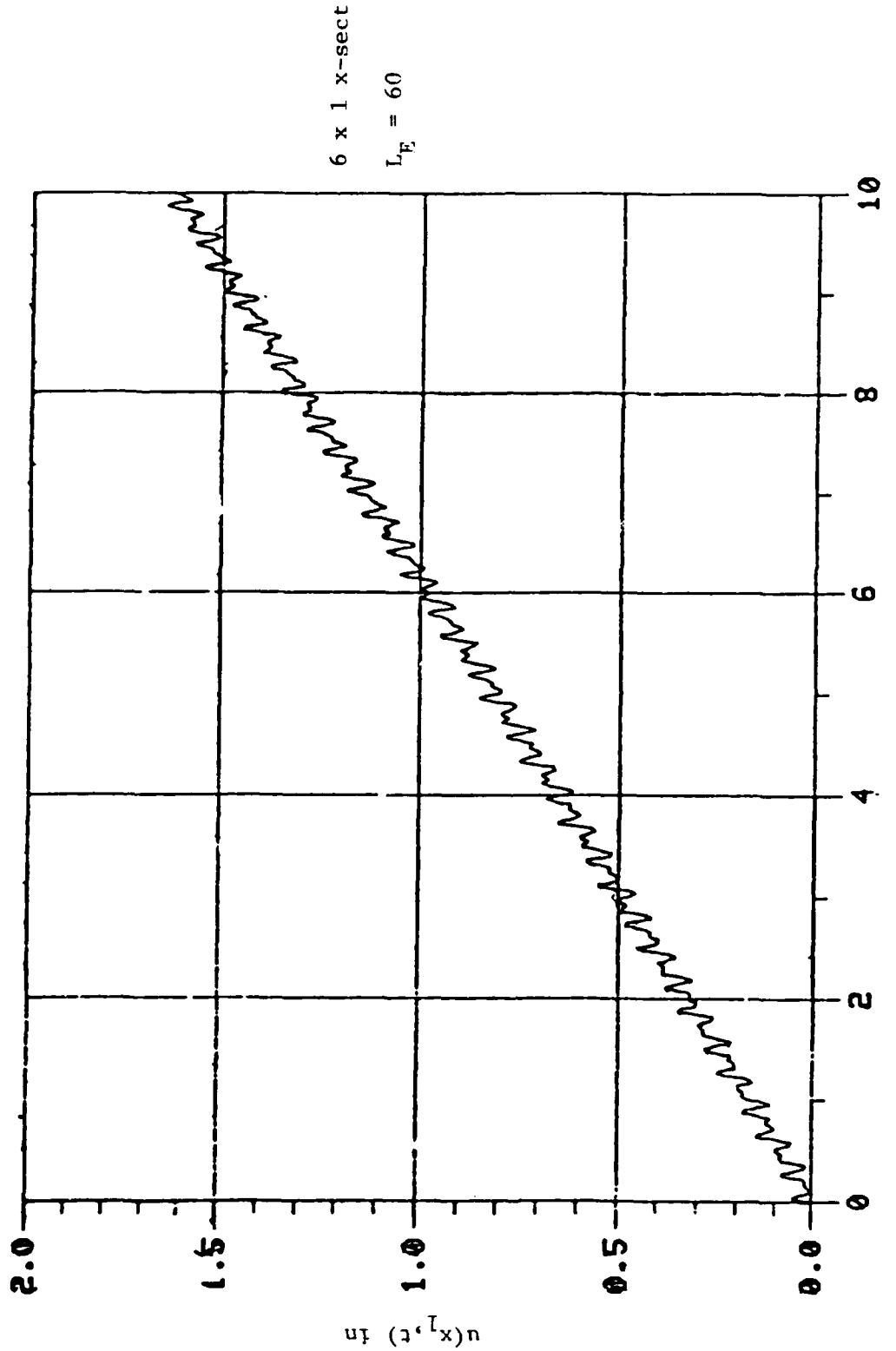


Figure 6. X-Displacement Plot at Node 1 for 6 x 1 X-Sect

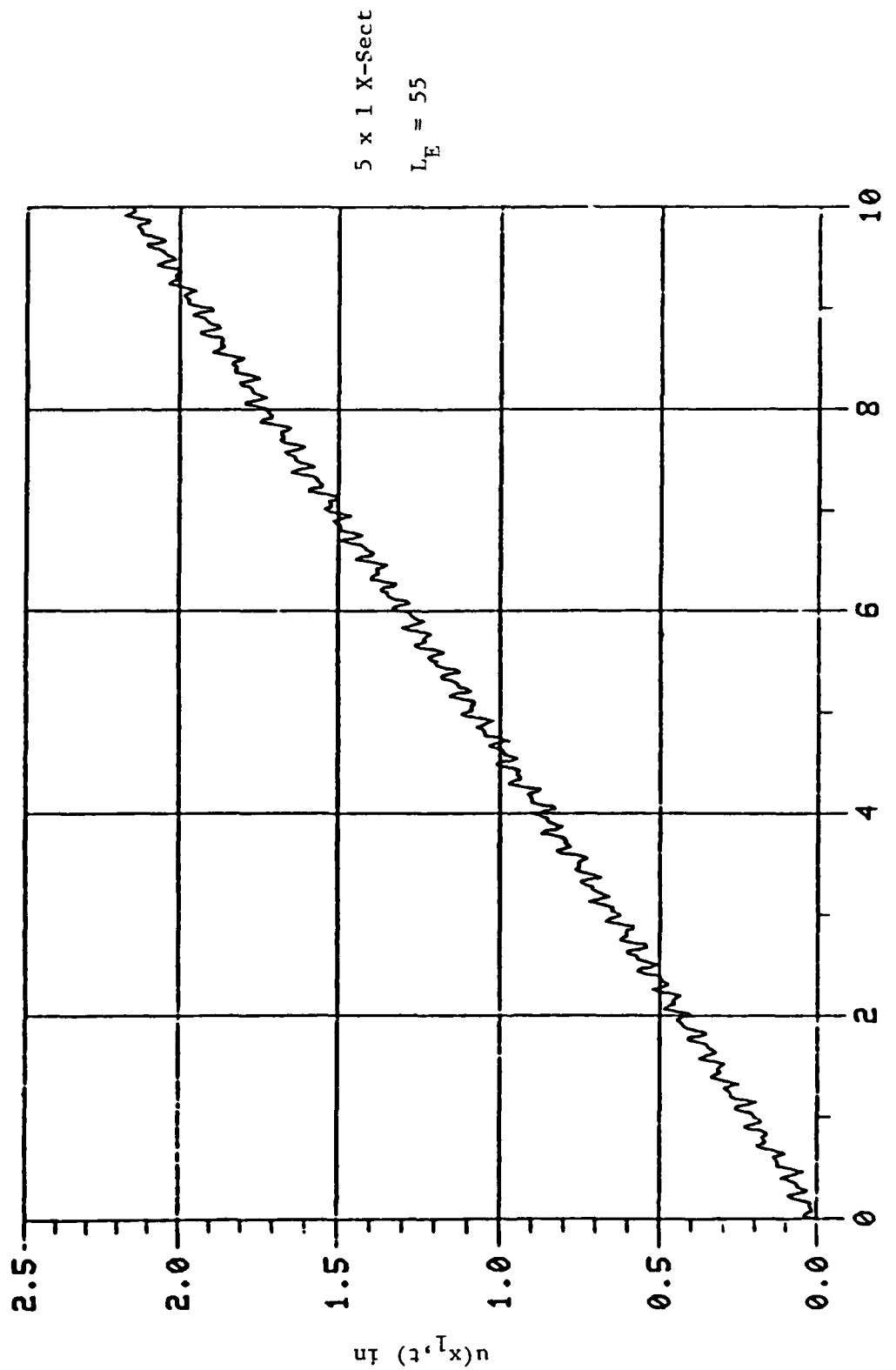


Figure 7. X-Displacement Plot at Node 1 for 5 x 1 Cross Section

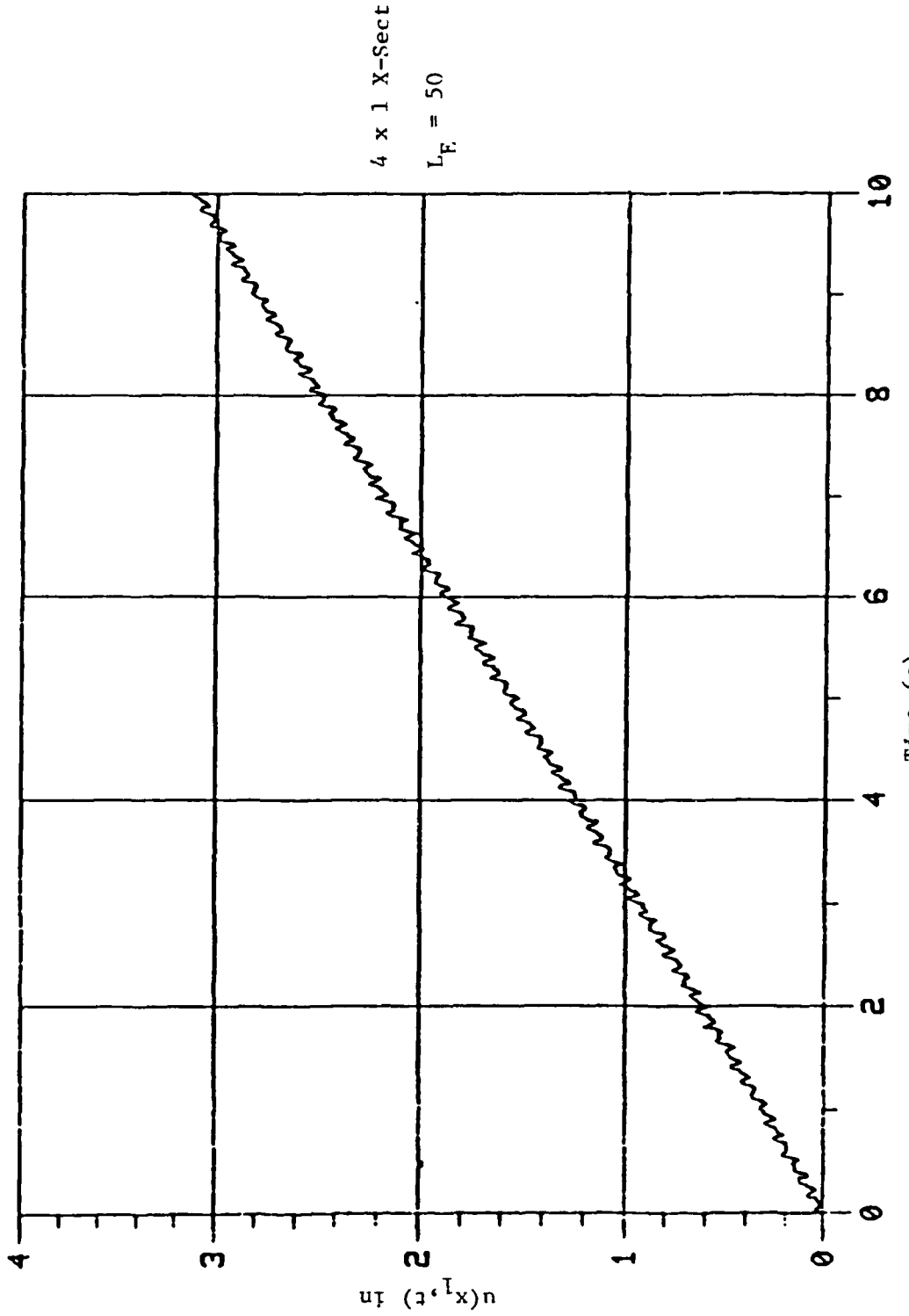


Figure 8. X-Displacement Plot at Node 1 for 4 x 1 Cross Section

A hinge assembly that connects the structure to the hanging cable from the ceiling is located at the midpoint of the horizontal beam. The cable will be 20 feet long to negate the pendulum motion of the structure. Half of this beam is taken as cantilevered. These two segments must have maximum rigidity designed in the z direction and significant structural flexibility in the x direction. One parallel beam and two thruster assemblies are attached to the free end of these segments. The static deflection in the z direction is set at 0.01 inch. For ease of construction, these segments have the same height as the parallel beams. The horizontal segment's width is varied to find the length and cross section that satisfy the static deflection criteria (see Table 3). The static deflection is computed using Equation (24) in which

$$P = 2(8) \text{ lbs} + W_{PARA}$$

where P denotes to the weight of the two thrusters and $W_{PARA}$ denotes the weight of one parallel beam. The length and cross section yielding the best combination of rigid-body and flexible-body modes in the response plot yield the design dimensions for the segment (see Figures 9 and 10). The horizontal beam is twice the length and has the same cross section of the segment. The third sizing criteria are to determine if torsional effects enter into the design set for the H-beam structure.

The model is tested to see if torsional modes can be excited by first testing to find the static angle of twist on the parallel beams. This $\Theta_{ST}$ results from the torque created by the weight of the thruster assembly. If $\Theta_{ST}$ is approximately equal to zero, the static angle of

Table 3. Calculating Length of Horizontal Segment for 2 Cross Sections

Example: 6" x 1" X-Sect (Al) Parallel Beams

$P = 2(8\ lb) + .585\ lb/in\ (2)(63\ in) = 90\ lb$

$$Z_{ST} = \frac{PL^3}{3EI} + \frac{qL^4}{8EI}$$

$I = 18\ in^4$ $E = 10 \times 10^6\ psi$

Horizontal Beam 6" x 1"

$$.01 = \frac{P(38)^3}{3(10x10^6)18} + \frac{.585(38)^4}{8(10x10^6)18} \qquad P = 90\ lb$$

Horizontal Beam 6" x 3"

$$.01 = \frac{P(51)^3}{3(10x10^6)54} + \frac{1.755(51)^4}{8(10x10^6)54} \qquad P = 90\ lb$$

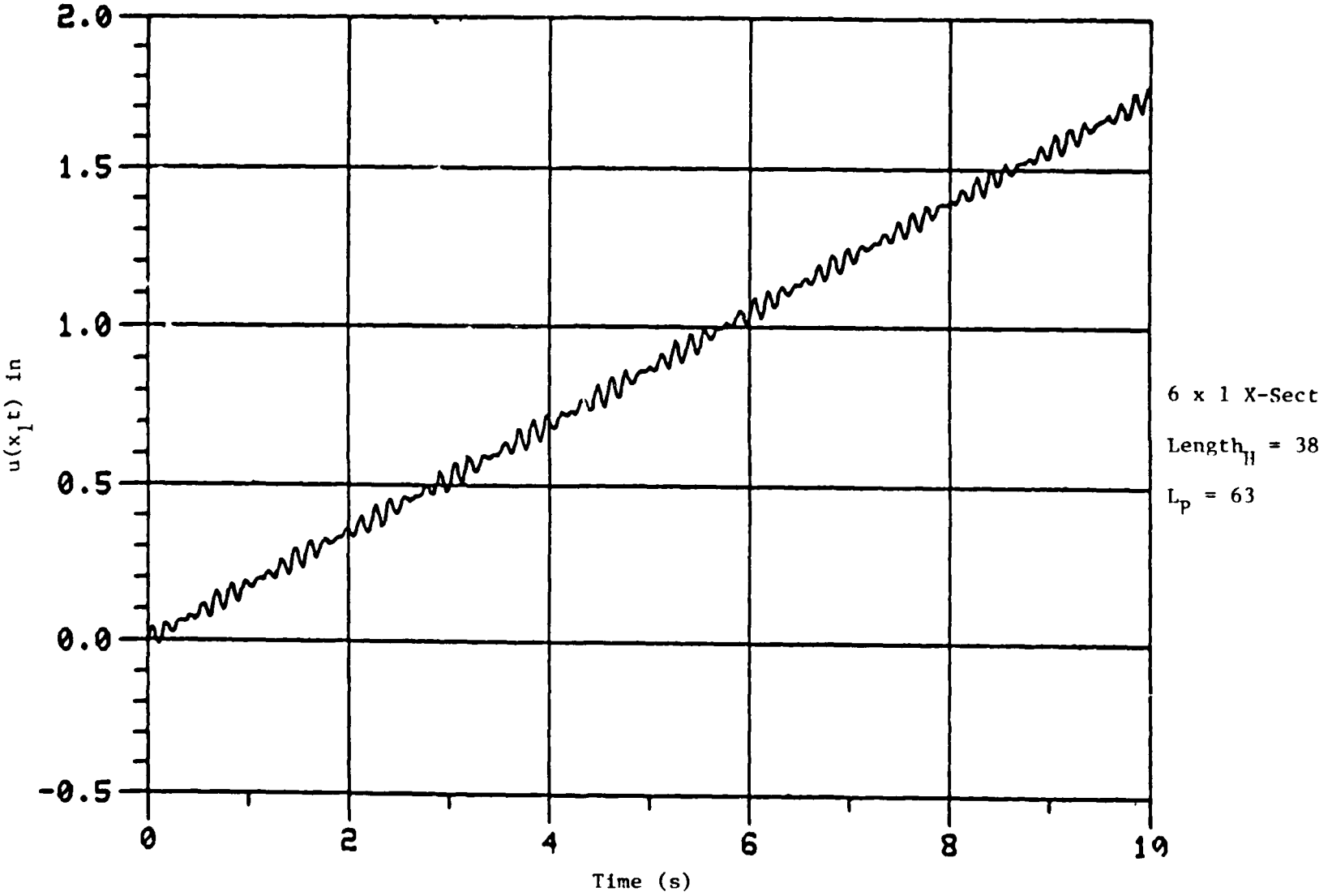


Figure 9. X-Displacement Plot at Node 1 for 6 x 1 Horizontal Beam Cross Section

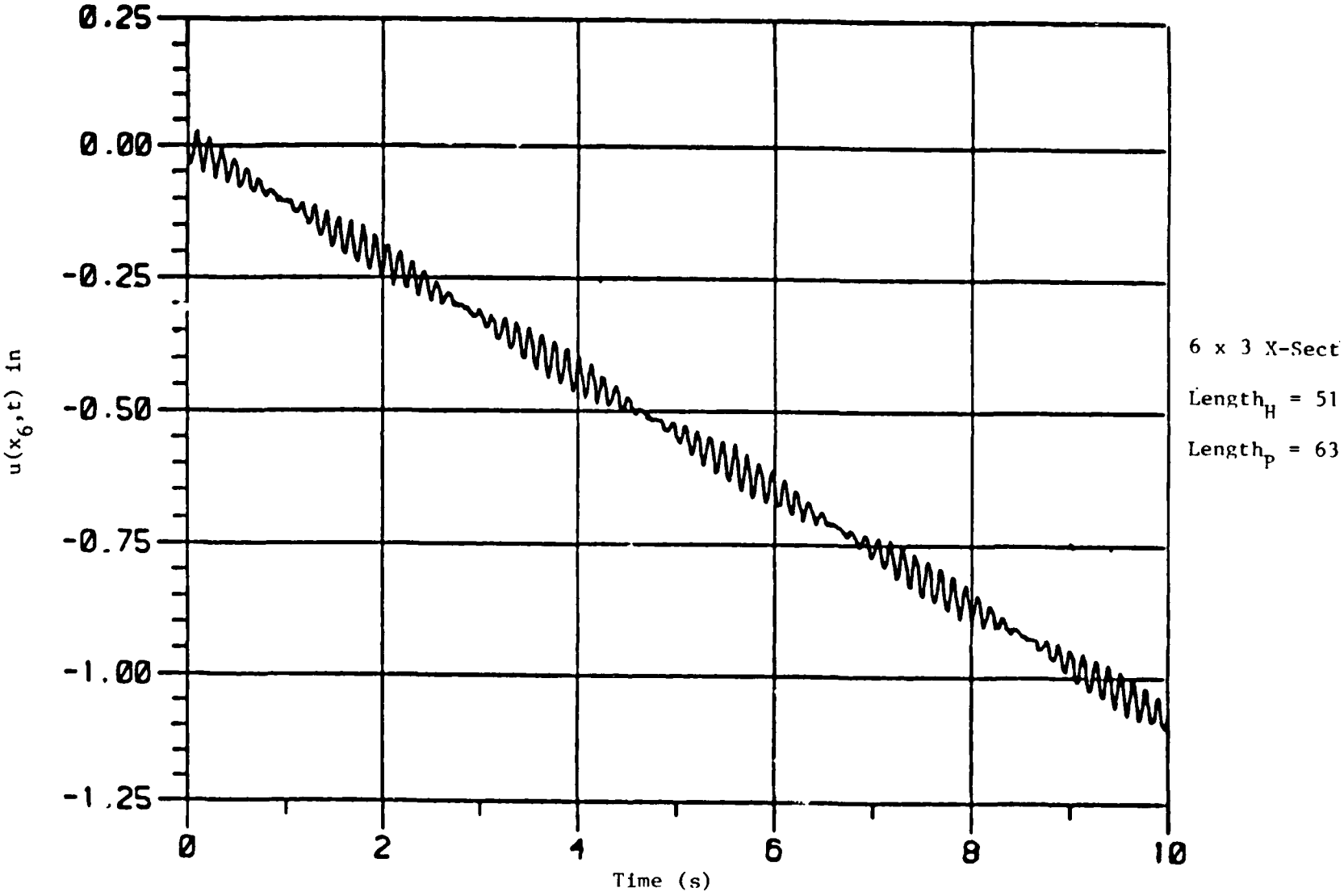


Figure 10. X-Displacement at Node 6 for 6 x 3 Horizontal Beam Cross Section

twist has virtually no effect on the structure. The static deflection for a cantilever beam in torsion is

$$\Theta_{ST} = \frac{TL}{GJ} \tag{25}$$

where T denotes the weight of a thruster assembly times the maximum perpendicular displacement $d_\perp$ of the assembly from the centroid of the beam's cross section, L represents the length of the segment, G denotes the beam's shear modulus, and J denotes the moment of inertia of the cross section. Next, the fundamental frequency of torsional response is computed to rate if this mode might be excited.

The torsion fundamental frequency $\omega_1$ is calculated for the designated parallel beam dimensions. The calculated frequency is compared with the first five modal frequencies that significantly contribute to the nodal response, and a torsional fundamental frequency significantly larger than these modal frequencies indicates that the structure will not be induced into torsional vibration as a result of the anticipated structural excitations. The torsional beam fundamental frequency is computed by

$$\omega_1 = \sqrt{\lambda_1} = \sqrt{\frac{GJ}{I}\beta^2} \qquad (r = 1) \tag{26}$$

where $\beta$ equals $r\pi/2L$ for a cantilever beam and I denotes the mass moment of inertia for the parallel beam cross section. The H-beam structure is evaluated to see if this torsional mode might be excited (see Table 4).

Table 4. Calculation Torsional $\Theta$ and $\omega_1$

Torsion

For a 6" x 1" X-Sect

$mg = 8$ lbs

$d = .5$ in

$G(Al) = 3.97 \times 10^6$ psi

$J = 18.5$ in$^4$

$L = 63$ in

$$\Theta_{ST} = \frac{TL}{GJ} = \frac{mg\ d\ L}{GJ}$$

$$= \frac{8(.5)63}{(3.97\times10^6)18.5}$$

$$= 3.43 \times 10^{-6} \text{ rad}$$

Find fundamental frequency

$$\lambda_r = \frac{GJ}{I}\beta^2 \qquad I = \frac{1}{12}(.0182 \text{ slug/in})(6^2 + 1^2)$$

$$\lambda_1 = \frac{3.97\times10^6(12)18.5}{\frac{1}{12}(.0182)(37)}\left(\frac{1(\pi)}{2(63)}\right)^2 = 9.76 \times 10^6 \text{ rad}^2/\text{s}^2 \qquad \beta = \frac{r\pi}{2L}$$

$$\omega_1 = 3124 \text{ rad/s}$$

# 4. HARDWARE CONSIDERATIONS

Next, the hardware necessary for the experimental set-up is considered. Structural dynamists and experimental test engineers at the NASA Langley Research Center in Hampton, Virginia, are consulted and they detail several requirements. The composition of the H-beam must be specified. In addition, certain design specifications are identified for the motors, sensors and actuators, and hinge assembly used as experimental equipment for this set-up.

## 4.1. Composition of Structure

An H-beam structure composed of aluminum is recommended because aluminum is light weight, one-third the weight of steel, and possesses excellent material properties. Several NASA Langley engineers mentioned that machinists favor aluminum because the metal is "easy" to machine. Welding properties of aluminum alloy 6061 are "first-rate." Since ease of construction is paramount in building the H-beam, aluminum is the choice for the structural composition.

## 4.2. Motors

When possible, DC permanent magnet motors should be used to power the sensors and actuators. Because these DC motors have only two wires, fewer wiring problems are incurred. Also, DC motors are easier to mount on a structure than AC motors. Motors come in torque drives, brush drives, and permanent magnet drive designs. Permanent magnet DC motors

have high reliability, long operational life, and require little maintenance. To power the air thrusters and sensors, 24-volt DC motors should be used.

## 4.3. Actuators or Thrusters

Thrusters are used for altitude control. Air thrusters are utilized on this experimental set-up. A thruster assembly is mounted at each end of the H-beam. The thrusters are positioned to fire in the x-y plane. Solenoid actuated cold gas jets provide the impulse forces. A compressed air tank supplies air to the jets via a flexible pressure hose running from the tank up to the ceiling, down the steel cable, and attached to the hinge assembly. The air passes through the hinge and through looped flexible hoses (Ref. 4) down to each thruster assembly which consists of four solenoid manifolds. Thus, the air leaves the flexible hose, goes through a four-way valve, and through short hoses to each of the manifolds. The manifolds gate the air flow between the regulated supply tank and the thrusters. Thrust is initiated with a discrete command that opens the solenoid. These thrusters will give an impulse force in the range of .6 lbs. On the next three pages are the examples of the type of thruster specifications desired (Tables 5, 6, and 7) (Ref. 2).

## 4.4. Sensors

For this experimental set-up, three types of sensors are required; position, rate, and acceleration. Position sensors detect x and y displacements and the theta angle between the displacements. Rate sensors

Table 5. Thruster Assembly Specifications

Thruster System (Example)

Thruster Manifold/Located near 3-DOF Hinge with 3/8-inch pipe thread to attach air hose

Thruster Assembly/Located at Nodes 1, 3, 4, and 6

Each Assembly Consists Of:

| | SPECS |
|---|---|
| Thruster Housing - 4 (see schematics) | 4 - 1/4" pipe treading (inlet)<br>4 - 1/8" pipe treading (outlet) |
| Solenoid Valve and Manifold - 4 | Coil rated - 24 VDC |
| Numatics Valve Assembly (on/off) (see schematics for wiring diagram for solenoids) | .25 Amps<br>6 watts<br>Operating time - .028 sec |
| Plumbing Flared Fittings - 4 | Standard |
| Air Hoses - 5 | Wall type 1 |
| - Parflex PE | Grade 4 |
| - Serial #QC44J22C1 | WP 125 psi<br>3/8 OD x .062 |

Valves - Rotary two-position type

Usable service from high vacuum to 300 psig with a nominal cutoff voltage of 0.4V

Table 6. Thruster Data

Typical Thruster Data (Example)

| | |
|---|---|
| Supply Pressure | 80 psi |
| Peak Thrust (Impulse) | 0.6 lb |
| Steady State Thrust | 0.3 lb |
| Duration of Thrust | 24 sec |

Table 7. Thruster Control Specifications

Thruster Control Design (Example)

Thruster Assembly at Each End of Structure (Nodes 1, 3, 4, 6)

| Type | Signal/Source | X-Coord | Y-Coord | Z-Coord | Sensitivity | Noise (mv rms) | Range | Bias |
|---|---|---|---|---|---|---|---|---|
| +x | DISC 1 | 12.5 | 21.0 | -127.3 | on/off | +0.0252 lb rms | 0.35 lbavg | 0 |
| -x | DISC 2 | " | " | " | on/off | +0.0252 lb rms | 0.35 lbavg | 0 |
| +y | DISC 3 | " | " | " | on/off | +0.0252 lb rms | 0.35 lbavg | 0 |
| -y | DISC 4 | " | " | " | on/off | +0.0252 lb rms | 0.35 lbavg | 0 |

detect either angular or displacement velocities, and acceleration sensors measure linear and angular acceleration (Ref. 5).

To detect linear position, rate, and acceleration, servo-accelerometers are advised for this set-up. The accelerometers are mounted as close to the thruster assemblies as possible. Rotational rate sensing units, rate gyros, detect angular position, rate, and acceleration and are suggested for this model. All sensors used on the model must have high response frequencies. A rate gyro attached to the bottom of the H-beam at the center of the structure will sense the H-beam going through rotations. On the next two pages are examples of recommended sensor control specifications (Tables 8 and 9)(Ref. 2).

## 4.5. Hinge Assembly

Attaching the structure to the steel cable hanging from the ceiling is a three degree-of-freedom hinge assembly. This assembly must easily support the weight of the H-beam, allow the structure to rotate about all three axes and translate in any two-dimensional plane. The hinge must also allow compressed air to be passed through it to the four looping flexing hoses. The three degree-of-freedom movement must still be possible. Some friction may result in the hinge because of the air-tight seals required in the assembly. This friction will increase the error of the data extracted from the model. A great deal of machining and precision engineering is necessary for such a complex design. According to Jeffery Williams, a NASA structural dynamisist who frequently uses hinge assemblies in his control of flexible structures experiments, a hinge of this standard costs in the range of $5-10 thousand.

Table 8. Accelerometer Control Specifications

Sensor Control Design (Example)

Accelerometers

| Type | Signal/Source | X-Coord | Y-Coord | Z-Coord | Sensitivity | Error | Range | Bias |
|---|---|---|---|---|---|---|---|---|
| Node 1X | ADC 0 | 7.0 | 15.8 | -129.3 | 0.0264 units/g | 0.17%F.S. | -20g | 0.00108V |
| Node 1Y | ADC 1 | 8.0 | 13.8 | -129.3 | 0.0284 units/g | 0.17%F.S. | -20g | 0.00066V |
| Node 3X | ADC 2 | 7.0 | 15.8 | -129.3 | 0.0264 units/g | 0.17%F.S. | -20g | 0.00105V |
| Node 3Y | ADC 3 | 8.0 | 13.8 | -129.3 | 0.0284 units/g | 0.17%F.S. | -20g | 0.00065V |
| Node 4X | ADC 4 | 7.0 | 15.8 | -129.3 | 0.0264 units/g | 0.17%F.S. | -20g | 0.00050V |
| Node 4Y | ADC 5 | 8.0 | 13.8 | -129.3 | 0.0284 units/g | 0.17%F.S. | -20g | 0.00077V |
| Node 6X | ADC 6 | 7.0 | 15.8 | -129.3 | 0.0264 units/g | 0.17%F.S. | -20g | 0.00103V |
| Node 6Y | ADC 7 | 8.0 | 13.8 | -129.3 | 0.0284 units/g | 0.17%F.S. | -20g | 0.00049V |

1 unit = 10 volts

F.S. = full scale

Table 9. Rate Gyro Control Specifications

Sensor Control Design (Example)

Rate Gyro

| Type | Signal/Source | X-Coord | Y-Coord | Z-Coord | Sensivity | Error | Range | Bias |
|---|---|---|---|---|---|---|---|---|
| Node 7 (roll) | ADC 8 | 27.8 | 0.0 | -5.3 | 0.0393 units/$s^{-1}$ | 3.6 deg/s rms | -360 (deg/s) | 2.458V |
| Node 7 (pitch) | ADC 9 | " | " | " | 0.2351 units/$s^{-1}$ | 0.55 deg/s rms | -60 (deg/s) | 2.361V |
| Node 7 (yaw) | ADC 10 | " | " | " | 0.2354 units/$s^{-1}$ | 0.50 deg/s rms | -60 (deg/s) | 2.564V |

# 5. RESULTS

After comparing the numerous test cases for the H-beam dimensions, the design choice is an H-beam with parallel beams four inches high, 3/8 inch thick, and 70 inches long, and a horizontal beam four inches high, 3/8 inch thick, and 58 inches long. This design shows excellent flexibility and easily supports the anticipated static loads, the weight of the sensors and the motors.

Checking the possibility of torsional excitation on the design proposed, $\Theta_{ST}$ and $\omega_1$ are

$$\Theta_{ST} = \frac{(12 \text{ lbs})(3/16 \text{ in})(35 \text{ in})}{(3.97 \times 10^6 \text{ lb/in}^2)(2.02 \text{ in}^4)} = 9.8 \times 10^{-6} \text{ rad}$$

$$\omega_1 = \sqrt{\frac{(3.97 \times 10^6 \text{ lb/in}^2)(12 \text{ in/ft})(2.02 \text{ in}^4)}{1/12(.004542 \text{ slug/in})(16.14 \text{ in}^2)} \left[\frac{1(\pi)}{2(35 \text{ in})}\right]^2} = 5632.9 \text{ rad/s.}$$

The static angle of twist is approxiamately equal to "zero" for this design even with a 12-lb thruster assembly. The torsional fundamental frequency is significantly greater than even the fifth natural frequency of the model. Therefore, torsional modes will not be induced for the structure proposed.

Further research of hinge assemblies concludes that the criteria set in this thesis is impractical. As previously stated, a hinge that allows compressed air to flow through it requires an immense quantity of engineering and cost. The hinge will have added friction resulting from the air seals on the hinge and will hinder motion causing a significant degree of error in the data extracted from this set-up. For cost and design effectiveness, a simple hinge that attaches the H-beam to the steel cable and a loosely wound flexible air hose to transport compressed air from the air

tank to the hoses on the structure are suggested. NASA aerodynamicists working in the Langley free-flight wind tunnel state the stiffness added to the model because of the compressed air in the hose is negligible.

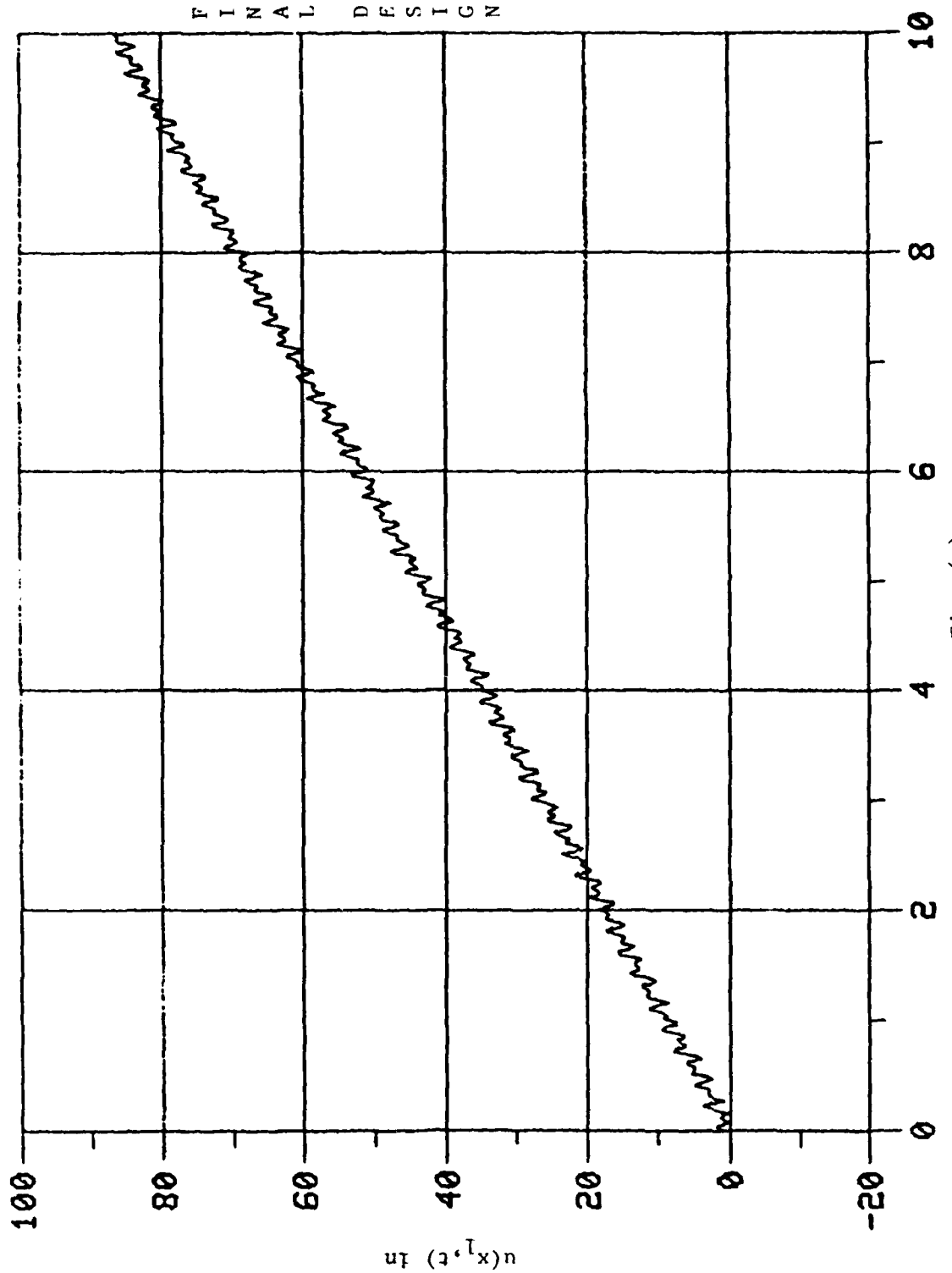


Figure 11. X-Displacement Plot at Node 1 for Final Design

# 6. CONCLUSION

A finite element is created to model a test article which will demonstrate control of flexible structures. The H-beam structure will have the dimensions, parallel beams, 4" x 3/8" x 70"; horizontal beam, 4" x 3/8" x 70". In addition, critical hardware specifications are mentioned for the motors, thrusters, and sensors. The hinge assembly proposed allows relatively free motion with errors due to added structural stiffness being negligible. In conclusion, an experimental set-up has successfully been designed to demonstrate flexible body maneuvers.

# 7. LIST OF REFERENCES


1. Meirovitch, L. Computational Methods in Structural Dynamics. Sijthoff and Noordhoff, The Netherlands, 1980.

2. Williams, J. and Rallo, R. Scole Users Manual. NASA Langley Research Center, Hampton, VA, February 1986.

3. Hutton, D. Applied Mechanical Vibrations. McGraw-Hill Book Company, NY, 1981.

4. Ford, H. Advanced Mechanics of Materials. John Wiley and Sons, Inc., NY, 1977.

5. Preliminary Flight Control Avionic Requirements for Orbiter-Attached Large Space Structures. Charles Stark Draper Laboratory, Inc., Cambridge, MA, January 1982.

6. Meirovitch, L. Elements of Vibration Analysis. McGraw-Hill Book Company, NY, 1975.

7. Meirovitch, L. Analytical Methods in Vibrations. Macmillan Company, London, 1967.

8. Noble, B. and Daniel, J. Applied Linear Algebra. Prentice-Hall, Inc., Englewood, NJ, 1977.

9. Lindeburg, M. Engineer in Training Review Manual. Professional Publications, San Carlos, CA, 1982.

10. Weaver, W. and Johnston, P. Finite Elements for Structural Analysis. Prentice-Hall, Inc., Englewood, NJ, 1984.

END

DATE

FILMED

FEB.

1988